



# Strong and highly conductive cellulose nanofibril/silver nanowires nanopaper for high performance electromagnetic interference shielding

Kun Liu<sup>1</sup> · Wei Liu<sup>1</sup> · Wei Li<sup>1</sup> · Yaxin Duan<sup>1</sup> · Keyu Zhou<sup>1</sup> · Shu Zhang<sup>1</sup> · Shuzhen Ni<sup>1,2</sup> · Ting Xu<sup>1,2</sup> · Haishun Du<sup>3</sup> · Chuanling Si<sup>1</sup>

Received: 3 January 2022 / Revised: 15 January 2022 / Accepted: 18 January 2022 / Published online: 15 February 2022  
© The Author(s), under exclusive licence to Springer Nature Switzerland AG 2022

## Abstract

Recently, the rapid popularization of modern communication technologies represented by 5G will inevitably aggravate the deterioration of the electromagnetic environment. Electromagnetic interference (EMI) and electromagnetic radiation have more and more serious impacts on human production and life, and EMI shielding materials have emerged as the times require. Herein, we reported a cellulose nanofibril/silver nanowire (CNF/AgNW) nanopaper, manufactured through a step-by-step (SbS) self-assembly process, which has a unique layered structure and improved two-sidedness. The results showed that the obtained AgNWs have an ultra-high aspect ratio (up to 2857), which enabled them to form conductive paths in nanopaper at low addition levels (0.5 wt.%). When the AgNW content was 5.0 wt.%, the obtained nanopaper with a thickness of ~ 50 µm exhibited an excellent tensile strength of ~ 98.6 MPa and a high conductivity of ~ 1673 S/cm. The unique layered structure of CNF/AgNW nanopaper and the excellent synergistic interaction between CNF and AgNWs enabled the optimized CNF/AgNW nanopaper to exhibit a high EMI shielding effectiveness (SE) of up to 67.27 dB in the X band. Therefore, this strong and highly conductive CNF/AgNW nanopaper is expected to broaden new application areas including smart clothing, wearable electronic devices, and other emerging applications.

**Keywords** Cellulose nanofibril · Silver nanowires · Cellulose nanopaper · Conductive films · EMI shielding

## 1 Introduction

With the rapid development of electronics industry, emerging electronic devices are widely used in human life [1–7]. While bringing convenience to people, electromagnetic

radiation pollution is inevitable. Many experiments have proved that long-term exposure to electromagnetic radiation will reduce human immunity and will cause irreversible effects in severe cases [8]. On the other hand, electromagnetic radiation will affect the normal working electronic equipment around it, and there is a huge risk for the precision equipment without shielding measures [9–12]. Nowadays, electromagnetic pollution has become a serious problem. The usage of electromagnetic interference (EMI) shielding materials has been considered as the main method to effectively eliminate the harm of electromagnetic waves [13]. Therefore, it is urgent to explore high-performance EMI shielding materials for human society, the ecological environment and even the economic and national defense construction.

Metals and metal alloy compounds possess high conductivity and are therefore widely used as traditional EMI shielding materials [14]. However, the poor flexibility, high density, difficulty in processing, and susceptibility to corrosion limit their applicability, especially in the field of

✉ Ting Xu  
xuting@tust.edu.cn

✉ Haishun Du  
hzd0024@auburn.edu

✉ Chuanling Si  
sichli@tust.edu.cn

<sup>1</sup> Tianjin Key Laboratory of Pulp and Paper, Tianjin University of Science and Technology, Tianjin 300457, China

<sup>2</sup> Key Laboratory of Pulp and Paper Science & Technology of Ministry of Education, Qilu University of Technology (Shandong Academy of Sciences), Jinan 250353, China

<sup>3</sup> Department of Chemical Engineering, Auburn University, Auburn, AL 36849, USA

portable and wearable devices [15]. In recent years, the fabrication of metal nanowires has received a great deal of attention due to the significantly improved properties (e.g., surface area, processability) [16]. Among them, silver nanowires (AgNWs) have become a promising candidate for EMI shielding application, considering their excellent characteristics of high aspect ratio, high specific surface area, good chemical stability, high electrical conductivity, and ease for mass production [17–19]. Nevertheless, AgNWs lack the ability to form mechanically robust self-assembly structures (e.g., films), which limited their practical applications. To solve this issue, AgNWs are widely applied as conductive coatings on different substrates or used as conductive nanofillers for a variety of polymeric matrix [20]. The obtained conductive AgNW/polymer composite films or foams have received extensive attention due to their good corrosion resistance, light weight, easy processing, and versatile designability [21]. However, most of these polymers are derived from petroleum-based materials, which face the problems of resource depletion and environmental pollution [22–25].

Cellulose is the most abundantly stored natural polymer compound on earth, with an annual output of about  $1.0 \times 10^{12}$  t [26–35]. It has the characteristics of low density, renewability, good biodegradability, and biocompatibility [36–47]. By physical or chemical means, cellulose can be processed into nanocellulose mainly including cellulose nanocrystal (CNC) and cellulose nanofibril (CNF) [48–53]. Compared to CNC, CNF has a higher aspect ratio and exhibits a significant tendency to form a three-dimensional network structure [54]. Thus, CNF has been widely used to produce flexible and mechanically robust cellulose nanopaper (CNP) through a self-assembly process (e.g., filtration, casting) [55]. Intriguingly, a variety of active materials such as conducting polymers, carbon nanomaterials, and metal nanomaterials can be compounded with the CNF through chemical or physical interactions, endowing the obtained CNP with multifunctional properties [27]. Therefore, the CNP composites have broad application prospects in the fields of flexible electronics, energy harvesting and conversion [33, 56], EMI shielding [57], energy storage [28, 58], biomedicines [59, 60], and so on [61–63].

Herein, we developed a step-by-step (SbS) assembly process for manufacturing a strong and highly conductive CNF/AgNW nanopaper with layered structure. CNF can facilitate the dispersion of AgNWs and interact with the AgNWs, resulting in relatively uniform distribution of AgNWs within the composite nanopaper. Therefore, a high conductivity of 1673.36 S/cm was achieved for the CNF/AgNW nanopaper with only 5.0 wt.% AgNWs. Since the AgNW surface was coated with a layer of polyvinylpyrrolidone (PVP), the interaction between AgNWs and CNF was significantly enhanced, resulting in the formation of the composite

nanostructure with high mechanical strength (~98.6 MPa). The layered structure of the composite nanopaper and the high electrical conductivity endow the CNF/AgNW nanopaper with high electromagnetic shielding performance (67.27 dB) even at a low thickness (~50  $\mu\text{m}$ ). The obtained CNF/AgNW nanopaper is expected to have broad application prospects in smart wearable electronics, national defense, aerospace, and so forth.

## 2 Materials and methods

### 2.1 Materials

The bleached softwood kraft pulp (BSKP) was provided by Shandong Taian Bai Chun Paper Co., Ltd., which contains  $79.1 \pm 0.2\%$  of glucan,  $15.2 \pm 0.5\%$  of xylan, and less than 0.1% of lignin. Formic acid (FA) (> 88.0%) was bought from Fuchen (Tianjin) Chemical Reagent Co., Ltd. Anhydrous ferric chloride ( $\text{FeCl}_3$ ) was purchased from Aladdin Reagent Co., Ltd. Silver nitrate ( $\text{AgNO}_3$ , > 99.8%) and was obtained from Sinopharm Chemical Reagent CO., Ltd. (Shanghai, China). Polyvinylpyrrolidone (PVP,  $M_w = 1.3 \times 10^6$ ) was purchased from Shanghai Macklin Biochemical Co., Ltd. Acetone was bought from Luoyang Haohua Chemical Reagent Co., China. Ethylene glycol (EG) was obtained from Tianjin Fuyu Fine Chemical Co., China. Sodium chloride (NaCl) and Sodium bromide (NaBr) were provided by Thermo Fisher Scientific (China) Co., Ltd.

### 2.2 Methods

#### 2.2.1 Fabrication of CNF

CNF aqueous suspension was produced from BSKP following the procedure we reported previously [27, 28]. Briefly, 20 g of BSKP and 1.2 g of  $\text{FeCl}_3$  were added into 600 mL 88% FA and hydrolyzed at 95 °C for 6 h. After that, the solid residue was washed to neutral pH and diluted with DI water to a concentration of 0.5 wt.%. Finally, the diluted suspension was subjected to a high-pressure homogenizer (AH-PILOT 2015, Antos Nanotechnology (Suzhou) Co., Ltd.) at a constant pressure of 100 MPa for ten times to obtain CNF.

#### 2.2.2 Fabrication of AgNWs

AgNWs were synthesized using a modified one-pot polyol method based on a previous report [17]. Firstly, 0.8 g of PVP was added to a three-necked flask containing 80 mL of EG, and the PVP was completely dissolved by magnetic stirring at 160 °C. Then, 20 mg of NaCl and 10 mg of NaBr were added, and the oxygen in the reaction system was removed

by flowing nitrogen gas. Finally, 40 mL of  $\text{AgNO}_3$  EG solution with a concentration of 0.02 g/mL was slowly added to the reaction system. After two minutes, both the stirring and the nitrogen flow were stopped. The reaction was left at 160 °C for 1.5 h, and the color of the reaction medium changed from white to gray green. The reaction mixture was cooled rapidly to room temperature in a cold-water bath. Twice the volume of acetone to the mixture was added, and the supernatant was removed when the solution comes out clearly delaminated. The lower precipitate was washed twice with ethanol and DI water by centrifugation (7000 rpm) to obtain pure AgNWs. The obtained AgNWs were dispersed in DI water for further use.

### 2.2.3 Fabrication of CNF/AgNW nanopaper

CNF/AgNW nanopaper was fabricated by SbS assembly method, as shown in Fig. 1. The CNF suspension was sonicated with a probe ultrasonicator at a power input of 300 W for 5 min. Then, a certain volume of AgNW suspension was mixed with CNF suspension, and magnetically stirred overnight to make them uniformly mixed. The mixture was used to manufacture CNF/AgNW nanopaper through vacuum filtration using a polypropylene filter membrane (diameter of 5 cm, pore size of 0.45  $\mu\text{m}$ ). Since the density of AgNWs is greater than that of CNF, if the mixture is filtered directly, AgNWs will be deposited on the bottom and layered with CNF, resulting in a serious two-sided difference in the obtained nanopaper. To avoid this problem, a SbS self-assembly method was adopted, i.e., filtering the mixture in batches. Take a portion of the mixture and add it to the suction filter bottle. After forming a thin film, slowly added an equal amount of the mixture to form another film on top of the previous one. Repeat the above steps until the mixture was completely used up. Finally, the wet CNF/AgNW nanopaper was placed between the two filter membranes and dried at 95 °C for 20 min to remove water. The obtained sample was labeled CNF/AgNWs-X, where X represented the mass percentage of AgNWs in the nanopaper. As a comparison, pure

CNF nanopaper was also obtained by the above SbS assembly process.

### 2.2.4 Characterization

Scanning electron microscope (SEM, JEOL-JSM IT300LV, Japan) was used to observe the morphology of AgNWs and the surface and cross-sectional morphology of the CNF/AgNW nanopaper. Transmission electron microscope (TEM, JEOL-JEM 2100 F, Japan) was used to observe the surface morphology of AgNWs in details. The chemical structures of CNF, AgNWs, PVP, and CNF/AgNW nanopaper were analyzed by FTIR-650 infrared spectrum analyzer in the wavelength range of 4000–400  $\text{cm}^{-1}$ . X-ray photoelectron spectroscopy (XPS) spectra of samples were collected on a photoelectron spectrometer (Thermo Scientific ESCALAB Xi+, America). The crystal structure of CNF, AgNWs and CNF/AgNW nanopaper were characterized by X-ray diffraction analyzer (XRD, Rigaku Smart lab, Japan) in the range of  $2\theta=5\text{--}70^\circ$  at a scanning rate of  $5^\circ \text{min}^{-1}$ .

Tensile tests of all nanopaper samples were measured by a 3360 universal material testing machine. The nanopaper samples were cut into 40 mm  $\times$  10 mm strips for tensile strength test at a speed of 2 mm/min. Each sample was tested three times to determine the average value.

The sheet resistance of the CNF/AgNW nanopaper was measured according to the van der Pauw four-point probe technique using a digital multimeter (KEITHLEY 2450). Before test, the nanopaper samples were cut into square specimens (15  $\times$  15  $\text{mm}^2$ ), and four corners of the specimen were coated with silver paint to ensure good electrical contacts. Then, the four probes were contacted on the four corners of the specimen and the resistance ( $R$ ) was recorded. The sheet resistance ( $R_s$ ) was calculated based on Eq. (1) [64], as follows:

$$R_s = \frac{\pi R}{\ln 2} \approx 4.53R \quad (1)$$

Further, the conductivity ( $\rho$ ) can be calculated from Eq. (2), as follows:

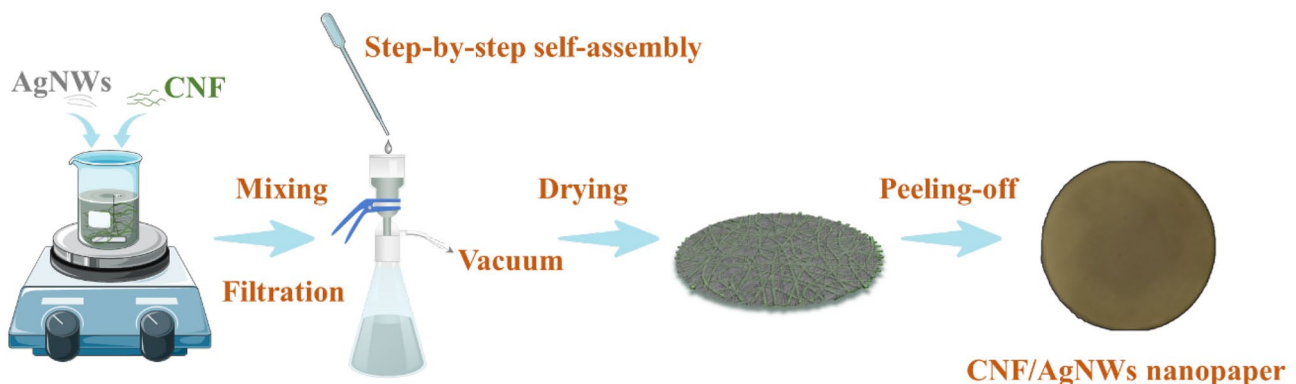


Fig. 1 Schematic illustration of the assembly process for the CNF/AgNW nanopaper

$$\rho = \frac{1}{R_s \times t} \quad (2)$$

where  $t$  is the thickness of the specimen. Three independent measurements were performed, and the averaged value was reported.

The EMI shielding performance of CNF/AgNW nanopapers were evaluated by a vector network analyzer (PNA-N5234A, Agilent, USA) in the frequency range of 8.2–12.4 GHz (X bands) based on a waveguide method. The total EMI shielding effectiveness ( $SE_T$ ), microwave reflection ( $SE_R$ ), and microwave absorption ( $SE_A$ ) can be obtained by the following equations:

$$SE_T = SE_R + SE_A + SE_M \quad (3)$$

$$SE_T = -10 \log \left( |S_{21}|^2 \right) \quad (4)$$

$$SE_R = -10 \log \left( 1 - |S_{11}|^2 \right) \quad (5)$$

$$SE_A = -10 \log \left( \frac{|S_{21}|^2}{1 - |S_{11}|^2} \right) \quad (6)$$

where  $S_{11}$  and  $S_{21}$  are the scattering parameters and  $SE_M$  is the microwave multiple internal reflection, which can be negligible when  $SE_T > 10$  dB [65].

### 3 Results and discussion

As shown in Fig. 2a–c, the obtained AgNWs display smooth surface, uniform length, and diameter distribution, and almost no silver nanoparticles can be observed. According to the statistics, the length and diameter of the AgNWs are about  $80 \pm 5 \mu\text{m}$  and  $28 \pm 3 \text{ nm}$ , respectively, indicating that the as-prepared AgNWs have a high aspect ratio (up to 2857). From Fig. 2b, we can notice that the tip of the AgNWs is relatively sharp, showing a pentagonal cross section. Meanwhile, it can be observed in Fig. 2b, c that the surface of AgNWs is wrapped by a thin layer of PVP with a thickness of about 1.2 nm, which can be proved by the FTIR analysis (Fig. 2d). All typical peaks of PVP can be observed in the FT-IR spectrum of the obtained AgNWs. Theoretically, Ag does not have infrared absorption peaks. However, the characteristic peak of PVP appeared in the infrared spectrum of the prepared AgNWs, indicating that the surface of AgNWs was wrapped with PVP [21]. The presence of PVP can effectively prevent the oxidation of AgNWs and

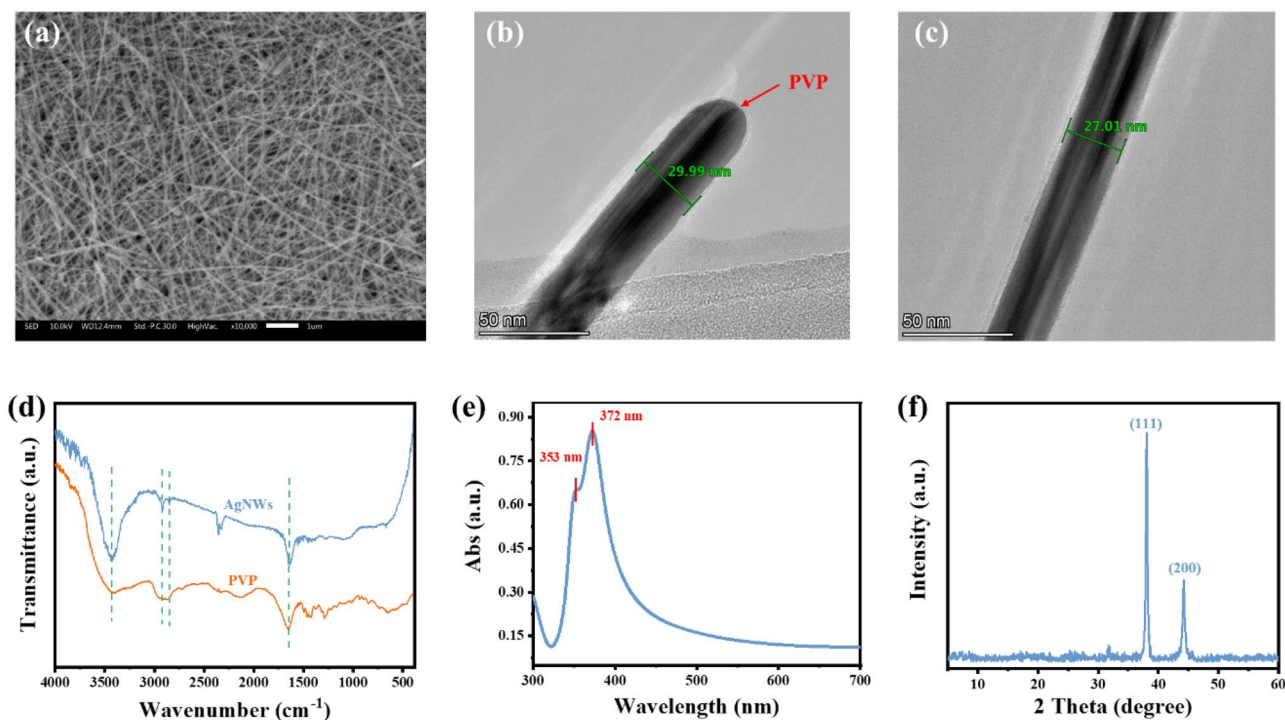


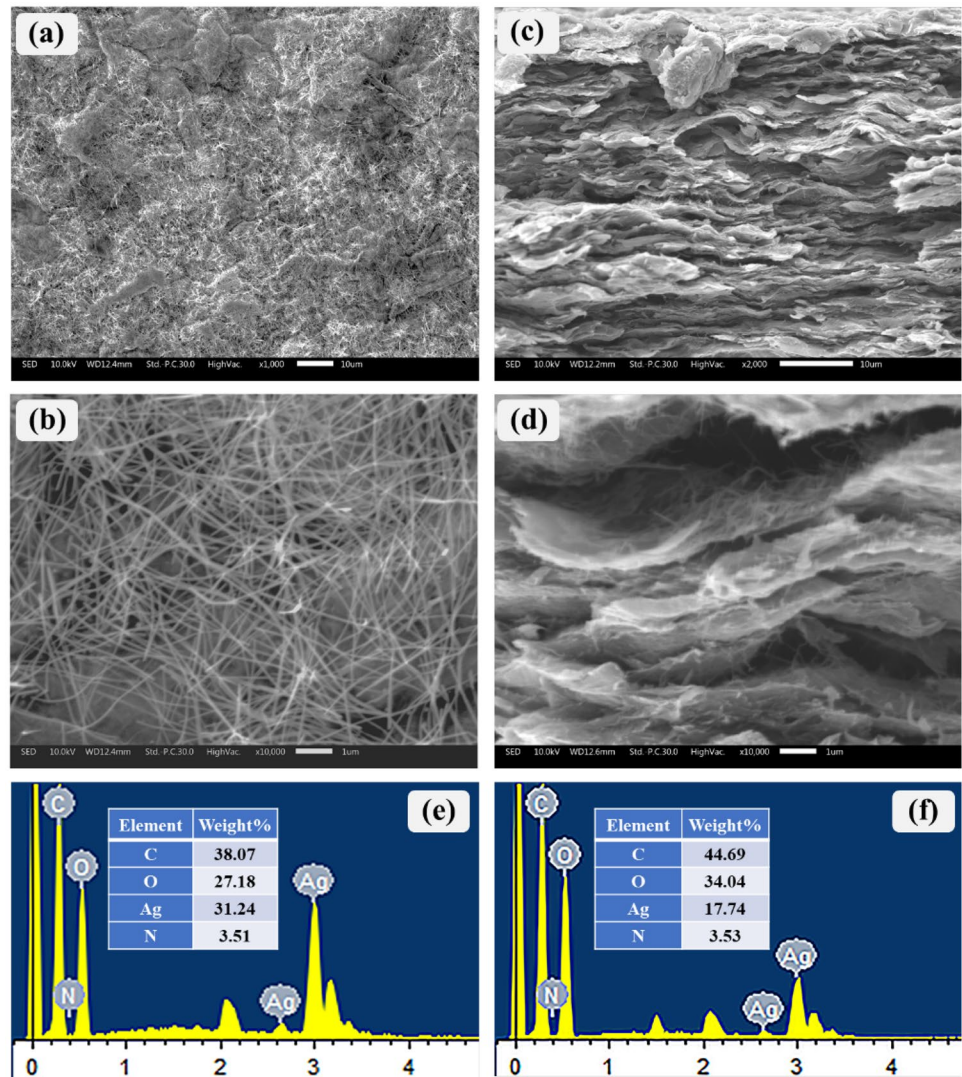
**Fig. 2** Characterization of AgNWs. (a) SEM. (b), (c) TEM images AgNWs. (d) FTIR spectra of AgNWs and PVP. (e) UV–Vis spectrum of AgNWs. (f) XRD pattern of AgNWs

increase the dispersion stability of AgNWs in water [66]. It should be noted that AgNWs are difficult to combine with other substances. The oxygen-containing functional groups in the PVP layer can form hydrogen bonds with the hydroxyl groups on the surface of CNF, which greatly increases the interface interaction between the AgNWs and CNF [67]. Figure 2e shows the UV–Vis spectrum of AgNWs, which is relatively smooth and without impurity peaks, indicating that the prepared AgNWs are of good quality. The peak at 353 nm corresponded to the longitudinal resonant peak of the one-dimensional AgNW pentagonal twin seed crystal, and the lateral characteristic peak at 372 nm was the characteristic peak of AgNWs [68]. As shown in Fig. 2f, the diffraction peaks of the AgNWs at  $2\theta = 38.28^\circ$ ,  $45.50^\circ$ , and  $64.80^\circ$  correspond to the (111), (200), and (220) crystal planes of silver, respectively [69]. Except for these diffraction peaks, no other impurity peaks can be observed, indicating that the synthesized AgNWs are composed of pure

surface cubic phase. The sharp peak shape with narrow half-width indicates the high crystallinity of the obtained AgNWs. In addition, as can be seen from Fig. 2f that the (111) crystal plane has the strongest diffraction peak (peak  $7595\text{ cm}^{-1}$ ), and its ratio to the diffraction peak intensity of (200) crystal plane (peak  $709\text{ cm}^{-1}$ ) reaches 3.1, which is higher than the theoretical value (2.5) [70]. This indicates that during the nucleation growth of the synthesized silver crystals, the growth rate of the (111) crystal plane is much higher than that of the other crystal planes, resulting in the growth of the material mainly in the one-dimensional direction, which leads to the generation of AgNWs [66]. All these results verify the high purity of the as-prepared AgNWs.

The surface and cross-sectional morphologies of CNF/AgNW nanopaper were characterized by SEM, as shown in Fig. 3 and Fig. S1. AgNWs can be clearly observed on the surface of nanopaper even at low content. For example, when the AgNW content was 0.5 wt.% (Fig. S1b), an interwoven AgNW network could

**Fig. 3** SEM and EDS spectra images of CNF/AgNWs-2.0wt.% surface (a, b, e) and cross-section (c, d, f)



be observed on the surface of the nanopaper. When the AgNW content increased to 5.0 wt.%, the surface (Fig. 3a, b, Fig. S1f) of the nanopaper was almost completely covered by AgNWs. More importantly, from the cross-sectional SEM images (Fig. 3c, d), a clear layered structure could be observed with AgNWs penetrating through it. This is due to the SbS self-assembly process and the strong interface between CNF and AgNW interaction. In addition, the EDS spectra images of the surface (Fig. 3e) and cross-section (Fig. 3f) of CNF/AgNWs-5.0 wt.% can further illustrate that AgNWs were uniformly distributed between layers of nanopaper.

In order to investigate the interaction between CNF and AgNWs in the CNF/AgNW nanopaper, FT-IR spectroscopy was performed. As shown in Fig. 4a, the CNF exhibited typical characteristic peaks of cellulose I $\beta$ , which was consistent with the previous results [71–73]. The peak at 1720 cm<sup>-1</sup> was attributed to the tensile vibration of C=O in the ester group on CNF [74]. Additionally, the characteristic peaks of CNF can be observed in all samples. However, with the increase of AgNW content, a blue shift of -OH group can be observed, and the characteristic peak intensity related to CNF decreased, which was attributed to the intermolecular hydrogen bond interaction between -OH in CNF and -C=O group in PVP wrapped on the surface of AgNWs (Fig. 4d). It is precisely because of this special intermolecular interaction

between CNF and PVP that AgNWs can be evenly and stably dispersed in the CNF suspension, which further ensured the uniform distribution of AgNWs within the composite nanopaper.

In addition, the crystalline structure of CNF/AgNW nanopaper with different AgNW content was analyzed by XRD (Fig. 4b, c). As shown in Fig. 4b, all samples exhibited the typical crystalline structure of cellulose and AgNWs. In the case of pure CNF, two main diffraction peaks are observed at  $2\theta = 16.2^\circ$  and  $22.5^\circ$ , corresponding to the (101) and (200) crystal planes of the typical crystal structure of cellulose I $\beta$  [75, 76]. With the addition of AgNWs, for all CNF/AgNW nanopaper samples, the characteristic peaks at  $2\theta = 38.28^\circ$ ,  $45.50^\circ$ , and  $64.80^\circ$  corresponding to the (111), (200), and (220) crystal planes of silver can be observed [69], which was consistent with the XRD results of the pure AgNWs (Fig. 2d). In addition to these peaks, there were no other new peaks, indicating that CNF/AgNW nanopaper was a composite composed of CNF and AgNWs without any other impurities. Moreover, the diffraction peak intensity related to CNF decreased with the increase of AgNW content, indicating that there was intermolecular interaction between CNF and AgNWs, which was consistent with the analysis results of FTIR.

Mechanical properties are of great significance to EMI shielding materials, especially in the field of wearable

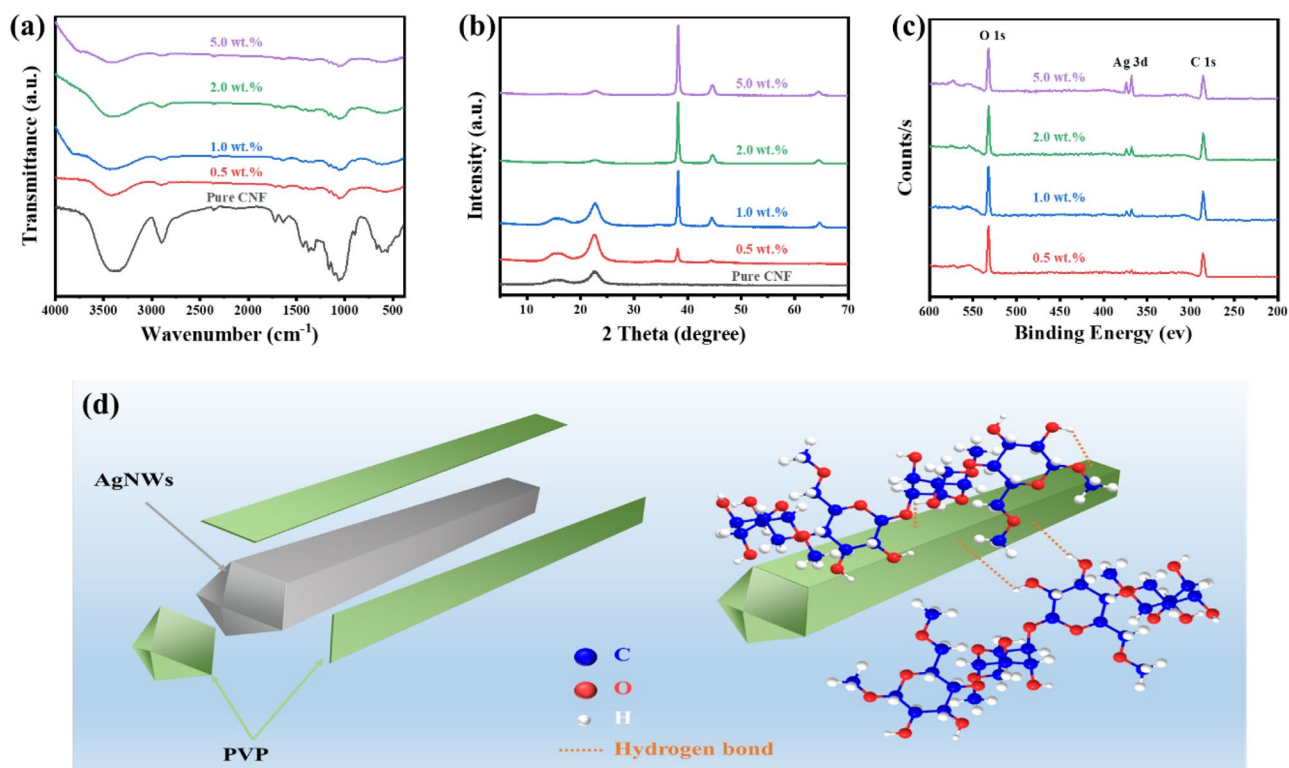


**Fig. 4** Characterization of CNF/AgNW nanopaper. (a) FTIR spectra. (b) XRD patterns. (c) XPS survey spectra. (d) Schematic diagram of the interaction between CNF and AgNWs

or portable electronic devices, which require sufficient strength and toughness to withstand mechanical deformation. Figure 5a and b show the stress–strain curve of nanopaper and the corresponding mechanical data. It can be seen that the pure CNF nanopaper exhibited the highest tensile strength (124.52 MPa) and breaking strain ( $\sim 9.1\%$ ). With the gradual increase of AgNW content, the tensile strength and breaking strain of CNF/AgNW nanopaper gradually decreased, which was mainly attributed to the relatively inactive surface of AgNWs. Compared with the strong interaction among CNF, the interaction between CNF and AgNWs was relatively weak. Even so, when the AgNW content was 5.0 wt.%, the nanopaper still showed a high tensile strength of  $\sim 98.6$  MPa, which was higher than most of those reported in the literature (Fig. S2). The main reason for such excellent mechanical performance is probably due to the uniform distribution of AgNWs within the composite nanopaper. In addition, the high aspect ratio of AgNWs and

the interactions between CNF and the AgNWs could be other factors [77, 78].

The conductivity of CNF/AgNW nanopaper with different content of AgNWs was further investigated, and the results are shown in Fig. 5c. In fact, the conductivity of pure CNF nanopaper is extremely low due to the insulating nature of cellulose. With a 0.5 wt.% addition of AgNWs, the conductivity of the CNF/AgNW nanopaper was greatly increased to 1615 S/cm, showing excellent conductivity. This is because AgNWs formed an interpenetrating conductive network on the surface and inside of the composite nanopaper (as shown in Fig. S1). With the continuous increase of AgNW content, the increase in conductivity of CNF/AgNW nanopaper gradually tends to be gentle. This is because once the conductive network is formed, too many AgNWs just form a repeated conductive network on this basis, resulting in limited conductivity improvement [21]. It can be seen that when the AgNW content was 5.0 wt.%, the conductivity of CNF/

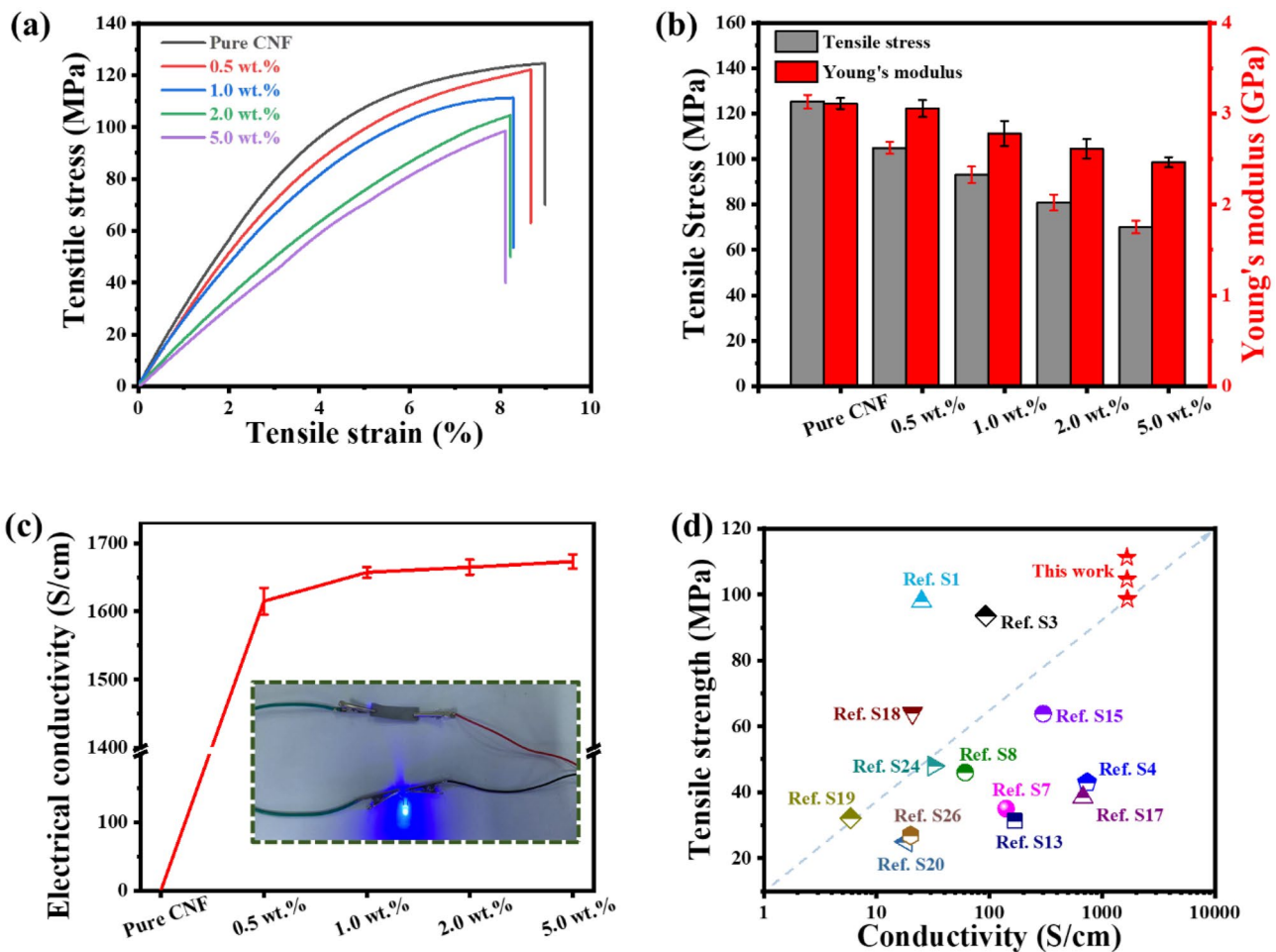


**Fig. 5** Mechanical and electrical properties of CNF/AgNW nanopaper: **(a)** Stress–strain curves. **(b)** The corresponding tensile strength and Young's modulus. **(c)** Electrical conductivity of CNF/AgNW nanopaper, the inset image exhibits the good electrical conductivity

of CNF/AgNW nanopaper. **(d)** Tensile strength and electrical properties of the CNF/AgNW nanopaper in comparison with those reported in the literature

AgNW nanopaper was 1673 S/cm, which was only about 60 S/cm higher than CNF/AgNWs-0.5 wt.%. In addition, the CNF/AgNWs-5.0 wt.% nanopaper also showed high conductivity in the thickness direction, indicating that a conductive channel overlapped by AgNWs was also formed in its vertical direction, which was consistent with the results observed in Fig. 2c, d. Through comparison (Fig. 5d, Table S1), it can be concluded that the CNF/AgNW nanopaper prepared in this work exhibited higher mechanical and electrical properties than those reported in other literatures, indicating considerable advantages in the practical application of electronic equipment or EMI shielding.

Figure 6a shows the EMI  $SE_T$  value of CNF/AgNW nanopaper in the X-band frequency range. It can be clearly seen that the EMI  $SE_T$  value of CNF/AgNW nanopaper had

a weak frequency dependence, and the EMI  $SE_T$  value of the entire X-band had a small difference, indicating that the composite nanopaper prepared by this method showed a wide working frequency band and stable shielding performance [79, 80]. When the AgNW content was only 0.5 wt.%, the EMI  $SE_T$  of CNF/AgNW nanopaper reached  $\sim 18$  dB. When the AgNW content was 1.0 wt.%, the EMI  $SE_T$  of CNF/AgNW nanopaper exceeded  $\sim 30$  dB, which was higher than the requirements of general commercial shielding materials [81]. When the AgNW content was 5.0 wt.%, the  $SE_T$  of nanopaper was as high as 67.26 dB, and the sample thickness was only  $\sim 50$   $\mu\text{m}$ . The increase in the loading of AgNWs made the surface and inside of the nanopaper produce a denser and more complete conductive network, which attenuated electromagnetic waves efficiently through

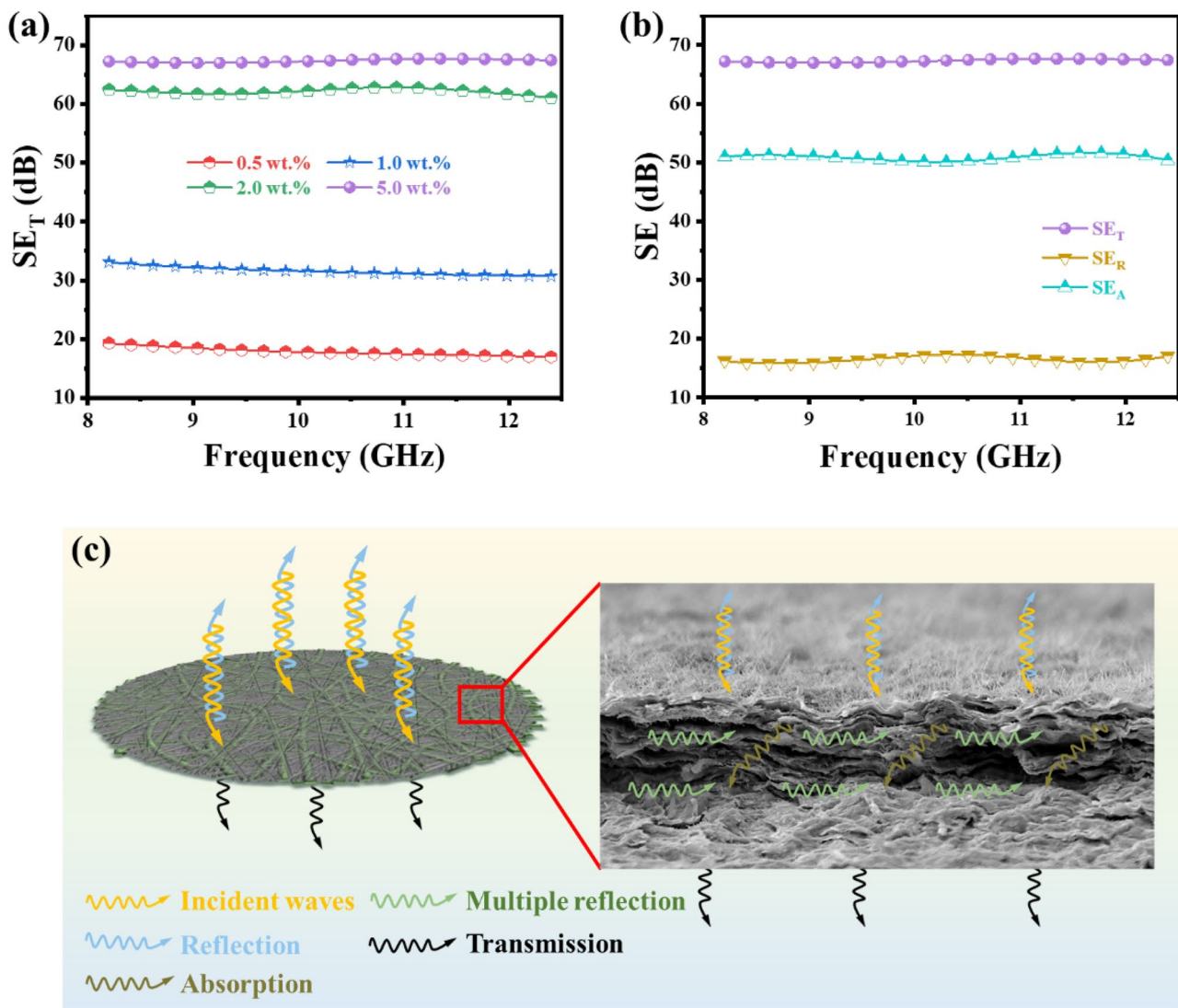


**Fig. 6** (a) EMI shielding performances of the CNF/AgNW nanopaper with different AgNW contents. (b) Comparison of  $SE_T$ ,  $SE_R$ ,  $SE_A$  of CNF/AgNW-5.0 wt.%. (c) Schematic diagram of EMI shielding mechanism of CNF/AgNW nanopaper



multiple reflections and absorptions. In addition, it can be found that the content of AgNWs had little effect on the conductivity increase of nanopaper (Fig. 5c), but significantly improved its  $SE_T$  value (Fig. 6a), which indicated that the EMI shielding performance depended not only on the conductivity of the composite, but also on the number of conductive channels, which was consistent with previous reports [9, 82]. In addition, the  $SE_T$ ,  $SE_A$ , and  $SE_R$  of CNF/AgNWs-5.0 wt.% were calculated and compared (Fig. 6b). Within the X band, the  $SE_T$ ,  $SE_A$ , and  $SE_R$  of CNF/AgNWs-5.0 wt.% were  $\sim 67.26$  dB,  $\sim 50.17$  dB, and  $\sim 17.09$  dB, respectively. It is obvious that  $SE_A$  made major contributions to the EMI  $SE_T$ . The high  $SE_A$  value was attributed to the conductive network formed on the surface and inside of the CNF/AgNW nanopaper and the interaction between CNF and AgNWs [15, 83, 84]. As shown in Fig. 6c, when the external incident electromagnetic wave contacted its surface, the highly conductive surface of CNF/AgNW nanopaper would immediately reflect part of the electromagnetic waves. Due to the special interlayer structure of CNF/AgNW nanopaper, most of the remaining electromagnetic waves would interact with the layered network structure composed of CNF and AgNWs in the interlayer of the nanopaper and converted them into heat energy, resulting in a large amount of microwave absorption and energy dissipation. Finally, after surface reflection, layer-by-layer absorption and energy dissipation, almost no electromagnetic waves could pass through the CNF/AgNW nanopaper. As shown in Table S2, the CNF/AgNW nanopaper in this work exhibited an amazing high EMI shielding performance even with the thickness of only  $\sim 50$   $\mu\text{m}$ , which was better than other materials reported in the literature.

## 4 Conclusions

In summary, the CNF/AgNW nanopaper with a typical layered structure was prepared through a SbS self-assembly process. Surprisingly, the as-prepared AgNWs has a super large aspect ratio (up to 2857), which can form an effective conductive network at a low content (e.g., 0.5 wt.%) in the CNF/AgNW nanopaper. Furthermore, given the low content of AgNWs in the nanopaper (5.0 wt.%) and the interfacial interaction between AgNWs and CNF, the electrical conductivity and EMI shielding performance in X-band of the layered CNF/AgNWs-5.0 wt.% nanopaper with a thickness of 50  $\mu\text{m}$  is 1673.36 S/cm and 67.26 dB, respectively. Importantly, it also exhibits excellent tensile strength (98.6 MPa). Overall, this work provides a facile and versatile approach for the fabrication of mechanically strong and highly conductive CNF/AgNW nanopaper with excellent EMI shielding performance, which has promising application prospects in the field of wearable or portable electronic devices.

**Supplementary information** The online version contains supplementary material available at <https://doi.org/10.1007/s42114-022-00425-2>.

**Funding** This work was supported by the National Natural Science Foundation of China (32071720), Tianjin Research Innovation Project for Postgraduate Students(2021YJSB198) and Foundation of Tianjin Key Laboratory of Pulp and Paper, Tianjin University of Science and Technology (202103). The project was also supported by the Foundation (No. KF202003) of Key Laboratory of Pulp and Paper Science & Technology of Ministry of Education of China. T. Xu thanks the China Postdoctoral Science Foundation (2021M702456). H. Du is financially supported by the China Scholarship Council (No.201708120052), and W. Liu is financially supported by the China Scholarship Council (No. 202108120056).

## Declarations

**Conflict of interest** The authors declare no competing interests.

## References

1. Yun T, Kim H, Iqbal A, Cho YS, Lee GS, Kim M-K, Kim SJ, Kim D, Gogotsi Y, Kim SO, Koo CM (2020) Electromagnetic shielding of monolayer MXene assemblies. *Adv Mater* 32(9):1906769. <https://doi.org/10.1002/adma.201906769>
2. Liu C, Huang Q, Zheng K, Qin J, Zhou D, Wang J (2020) Impact of lithium salts on the combustion characteristics of electrolyte under diverse pressures. *Energies* 13(20):5373. <https://doi.org/10.3390/en13205373>
3. Liu C, Zheng K, Zhou Y, Zhu K, Huang Q (2021) Experimental thermal hazard investigation of pressure and EC/PC/EMC mass ratio on electrolyte. *Energies* 14(9):2511. <https://doi.org/10.3390/en14092511>
4. Liu C, Xu D, Weng J, Zhou S, Li W, Wan Y, Jiang S, Zhou D, Wang J, Huang Q (2020) Phase change materials application in battery thermal management system: a review. *Materials* 13(20):4622. <https://doi.org/10.3390/ma13204622>
5. Tan L, Wei C, Zhang Y, An Y, Xiong S, Feng J (2022) Long-life and dendrite-free zinc metal anode enabled by a flexible, green and self-assembled zincophilic biomass engineered MXene based interface. *Chem Eng J* 431:134277. <https://doi.org/10.1016/j.cej.2021.134277>
6. Liu S, Du H, Liu K, Ma M, Kwon Y-E, Si C, Ji X, Choi S-E, Zhang X (2021) Flexible and porous  $\text{Co}_3\text{O}_4$ -carbon nanofibers as binder-free electrodes for supercapacitors. *Adv Compos Hybrid Mater* 4(4):1367–1383. <https://doi.org/10.1007/s42114-021-00344-8>
7. Xiong R, Xu RX, Huang C, Smedt SD, Braeckmans K (2021) Stimuli-responsive nanobubbles for biomedical applications. *Chem Soc Rev* 50(9):5746–5776. <https://doi.org/10.1039/C9CS00839J>
8. Zhang Y, Cheng W, Tian W, Lu J, Song L, Liew KM, Wang B, Hu Y (2020) Nacre-inspired tunable electromagnetic interference shielding sandwich films with superior mechanical and fire-resistant protective performance. *ACS Appl Mater Interfaces* 12(5):6371–6382. <https://doi.org/10.1021/acsami.9b18750>
9. Zhou Z, Liu J, Zhang X, Tian D, Zhan Z, Lu C (2019) Ultrathin MXene/calcium alginate aerogel film for high-performance electromagnetic interference shielding. *Adv Mater Interfaces* 6(6):1802040. <https://doi.org/10.1002/admi.201802040>
10. Asmatulu R, Bollavaram PK, Patlolla VR, Alarifi IM, Khan WS (2020) Investigating the effects of metallic submicron and nanofilms on fiber-reinforced composites for lightning strike protection

- and EMI shielding. *Adv Compos Hybrid Mater* 3(1):66–83. <https://doi.org/10.1007/s42114-020-00135-7>
11. Gao Q, Pan Y, Zheng G, Liu C, Shen C, Liu X (2021) Flexible multilayered MXene/thermoplastic polyurethane films with excellent electromagnetic interference shielding, thermal conductivity, and management performances. *Adv Compos Hybrid Mater* 4(2):274–285. <https://doi.org/10.1007/s42114-021-00221-4>
  12. Wang Y, Wang P, Du Z, Liu C, Shen C, Wang Y (2021) Electromagnetic interference shielding enhancement of poly(lactic acid)-based carbonaceous nanocomposites by poly(ethylene oxide)-assisted segregated structure: a comparative study of carbon nanotubes and graphene nanoplatelets. *Adv Compos Hybrid Mater*. <https://doi.org/10.1007/s42114-021-00320-2>
  13. Liu R, Miao M, Li Y, Zhang J, Cao S, Feng X (2018) Ultrathin biomimetic polymeric  $\text{Ti}_3\text{C}_2\text{T}_x$  MXene composite films for electromagnetic interference shielding. *ACS Appl Mater Interfaces* 10(51):44787–44795. <https://doi.org/10.1021/acsami.8b18347>
  14. Zeng Z, Wang C, Siqueira G, Han D, Huch A, Abdolhosseinzadeh S, Heier J, Nüesch F, Zhang C, Nyström G (2020) Nanocellulose-MXene biomimetic aerogels with orientation-tunable electromagnetic interference shielding performance. *Adv Sci* 7(15):2000979. <https://doi.org/10.1002/advs.202000979>
  15. Ma C, Cao W, Zhang W, Ma M, Sun W, Zhang J, Chen F (2021) Wearable, ultrathin and transparent bacterial celluloses/MXene film with Janus structure and excellent mechanical property for electromagnetic interference shielding. *Chem Eng J* 403:126438. <https://doi.org/10.1016/j.cej.2020.126438>
  16. Choi HY, Lee T-W, Lee S-E, Lim J, Jeong YG (2017) Silver nanowire/carbon nanotube/cellulose hybrid papers for electrically conductive and electromagnetic interference shielding elements. *Compos Sci Technol* 150:45–53. <https://doi.org/10.1016/j.compscitech.2017.07.008>
  17. Chen Y, Pang L, Li Y, Luo H, Duan G, Mei C, Xu W, Zhou W, Liu K, Jiang S (2020) Ultra-thin and highly flexible cellulose nanofiber/silver nanowire conductive paper for effective electromagnetic interference shielding. *Compos Part Appl Sci Manuf* 135:105960. <https://doi.org/10.1016/j.compositesa.2020.105960>
  18. Cheng H, Pan Y, Chen Q, Che R, Zheng G, Liu C, Shen C, Liu X (2021) Ultrathin flexible poly(vinylidene fluoride)/MXene/silver nanowire film with outstanding specific EMI shielding and high heat dissipation. *Adv Compos Hybrid Mater* 4:505–513. <https://doi.org/10.1007/s42114-021-00224-1>
  19. Huang K, Liu J, Lin S, Wu Y, Chen E, He Z, Lei M (2021) Flexible silver nanowire dry electrodes for long-term electrocardiographic monitoring. *Adv Compos Hybrid Mater*. <https://doi.org/10.1007/s42114-021-00322-0>
  20. Yang S, Yan D, Li Y, Lei J, Li Z (2021) Flexible poly(vinylidene fluoride)-MXene/silver nanowire electromagnetic shielding films with joule heating performance. *Ind Eng Chem Res* 60(27):9824–9832. <https://doi.org/10.1021/acs.iecr.1c01632>
  21. Yin R, Yang S, Li Q, Zhang S, Liu H, Han J, Liu C, Shen C (2020) Flexible conductive Ag nanowire/cellulose nanofibril hybrid nanopaper for strain and temperature sensing applications. *Sci Bull* 65(11):899–908. <https://doi.org/10.1016/j.scib.2020.02.020>
  22. Xu D, Huang G, Guo L, Chen Y, Ding C, Liu C (2021) Enhancement of catalytic combustion and thermolysis for treating polyethylene plastic waste. *Adv Compos Hybrid Mater*. <https://doi.org/10.1007/s42114-021-00317-x>
  23. Li X, Lu X, Nie S, Liang M, Yu Z, Duan B, Yang J, Xu R, Lu L, Si C (2020) Efficient catalytic production of biomass-derived levulinic acid over phosphotungstic acid in deep eutectic solvent. *Ind Crops Prod* 145:112154. <https://doi.org/10.1016/j.indcrop.2020.112154>
  24. Liu R, Dai L, Xu C, Wang K, Zheng C, Si C (2020) Lignin-based micro- and nanomaterials and their composites in biomedical applications. *Chemsuschem* 13(17):4266–4283. <https://doi.org/10.1002/cssc.202000783>
  25. Xu J, Li C, Dai L, Xu C, Zhong Y, Yu F, Si C (2020) Biomass fractionation and lignin fractionation towards lignin valorization. *Chemsuschem* 13(17):4284–4295. <https://doi.org/10.1002/cssc.202001491>
  26. An L, Si C, Wang G, Sui W, Tao Z (2019) Enhancing the solubility and antioxidant activity of high-molecular-weight lignin by moderate depolymerization via in situ ethanol/acid catalysis. *Ind Crops Prod* 128:177–185. <https://doi.org/10.1016/j.indcrop.2018.11.009>
  27. Du H, Parit M, Liu K, Zhang M, Jiang Z, Huang T-S, Zhang X, Si C (2021) Multifunctional cellulose nanopaper with superior water-resistant, conductive, and antibacterial properties functionalized with chitosan and polypyrrole. *ACS Appl Mater Interfaces* 13(27):32115–32125. <https://doi.org/10.1021/acsami.1c06647>
  28. Du H, Zhang M, Liu K, Parit M, Jiang Z, Zhang X, Li B, Si C (2022) Conductive PEDOT:PSS/cellulose nanofibril paper electrodes for flexible supercapacitors with superior areal capacitance and cycling stability. *Chem Eng J* 428:131994. <https://doi.org/10.1016/j.cej.2021.131994>
  29. Liu K, Du H, Zheng T, Liu W, Zhang M, Liu H, Zhang X, Si C (2021) Lignin-containing cellulose nanomaterials: preparation and applications. *Green Chem* 23(24):9723–9746. <https://doi.org/10.1039/D1GC02841C>
  30. Liu H, Xu T, Liu K, Zhang M, Liu W, Li H, Du H, Si C (2021) Lignin-based electrodes for energy storage application. *Ind Crops Prod* 165:113425. <https://doi.org/10.1016/j.indcrop.2021.113425>
  31. Sun L, Zhang X, Liu H, Liu K, Du H, Kumar A, Sharma G, Si C (2021) Recent advances in hydrophobic modification of nanocellulose. *Curr Org Chem* 25(3):417–436. <https://doi.org/10.2174/1385272824999201210191041>
  32. Xu T, Du H, Liu H, Liu W, Zhang X, Si C, Liu P, Zhang K (2021) Advanced nanocellulose-based composites for flexible functional energy storage devices. *Adv Mater* 33(48):2101368. <https://doi.org/10.1002/adma.202101368>
  33. Zhang M, Du H, Liu K, Nie S, Xu T, Zhang X, Si C (2021) Fabrication and applications of cellulose-based nanogenerators. *Adv Compos Hybrid Mater* 4:865–884. <https://doi.org/10.1007/s42114-021-00312-2>
  34. Chen S, Wang G, Sui W, Parvez AM, Dai L, Si C (2020) Novel lignin-based phenolic nanosphere supported palladium nanoparticles with highly efficient catalytic performance and good reusability. *Ind Crops Prod* 145:112164. <https://doi.org/10.1016/j.indcrop.2020.112164>
  35. Li X, Xu R, Yang J, Nie S, Liu D, Liu Y, Si C (2019) Production of 5-hydroxymethylfurfural and levulinic acid from lignocellulosic biomass and catalytic upgradation. *Ind Crops Prod* 130:184–197. <https://doi.org/10.1016/j.indcrop.2018.12.082>
  36. Liu W, Du H, Liu K, Liu H, Xie H, Si C, Pang B, Zhang X (2021) Sustainable preparation of cellulose nanofibrils via choline chloride-citric acid deep eutectic solvent pretreatment combined with high-pressure homogenization. *Carbohydr Polym* 267:118220. <https://doi.org/10.1016/j.carbpol.2021.118220>
  37. Liu H, Du H, Zheng T, Liu K, Ji X, Xu T, Zhang X, Si C (2021) Cellulose based composite foams and aerogels for advanced energy storage devices. *Chem Eng J* 426:130817. <https://doi.org/10.1016/j.cej.2021.130817>
  38. Liu H, Liu K, Han X, Xie H, Si C, Liu W, Bae Y (2020) Cellulose nanofibrils-based hydrogels for biomedical applications: progresses and challenges. *Curr Med Chem* 27(28):4622–4646. <https://doi.org/10.2174/0929867327666200303102859>
  39. Wang H, Du H, Liu K, Liu H, Xu T, Zhang S, Chen X, Zhang R, Li H, Xie H, Zhang X, Si C (2021) Sustainable preparation of bifunctional cellulose nanocrystals via mixed  $\text{H}_2\text{SO}_4$ /formic acid

- hydrolysis. *Carbohydr Polym* 266(15):118107. <https://doi.org/10.1016/j.carbpol.2021.118107>
40. Liu W, Du H, Zheng T, Si C (2021) Recent insights on biomedical applications of bacterial cellulose based composite hydrogels. *Curr Med Chem*. <https://doi.org/10.2174/0929867328666210412124444>
  41. Liu W, Du H, Zhang M, Liu K, Liu H, Xie H, Zhang X, Si C (2020) Bacterial cellulose-based composite scaffolds for biomedical applications: a review. *ACS Sustain Chem Eng* 8(20):7536–7562. <https://doi.org/10.1021/acssuschemeng.0c00125>
  42. Dai L, Cao Q, Wang K, Han S, Si C, Liu D, Liu Y (2020) High efficient recovery of L-lactide with lignin-based filler by thermal degradation. *Ind Crops Prod* 143:111954. <https://doi.org/10.1016/j.indcrop.2019.111954>
  43. Xu R, Si C, Kong F, Li X (2020) Synthesis of  $\gamma$ -valerolactone and its application in biomass conversion. *J For Eng* 5(2):20–28. <https://doi.org/10.13360/j.issn.2096-1359.201904004>
  44. Yang J, Si C, Liu K, Liu H, Li X and Liang M (2020) Production of levulinic acid from lignocellulosic biomass and application. *J For Eng* 5(5): 21–27. <https://doi.org/10.13360/j.issn.2096-1359.201905013>
  45. Xie Z, Tian Z, Liu S, Ma H, Ji X, Si C (2022) Effects of different amounts of cellulase on the microstructure and soluble substances of cotton stalk bark. *Adv Compos Hybrid Mater*. <https://doi.org/10.1007/s42114-021-00400-3>
  46. Xu R, Du H, Liu C, Liu H, Wu M, Zhang X, Si C, Li B (2021) An efficient and magnetic adsorbent prepared in a dry process with enzymatic hydrolysis residues for wastewater treatment. *J Clean Prod* 313:127834. <https://doi.org/10.1016/j.jclepro.2021.127834>
  47. Wang Y, Ji X, Liu S, Tian Z, Si C, Wang R, Yang G, Wang D (2022) Effects of two different enzyme treatments on the microstructure of outer surface of wheat straw. *Adv Compos Hybrid Mater*. <https://doi.org/10.1007/s42114-021-00395-x>
  48. Du H, Parit M, Liu K, Zhang M, Jiang Z, Huang T-S, Zhang X, Si C (2021) Engineering cellulose nanopaper with water resistant, antibacterial, and improved barrier properties by impregnation of chitosan and the followed halogenation. *Carbohydr Polym* 270:118372. <https://doi.org/10.1016/j.carbpol.2021.118372>
  49. Liu K, Du H, Liu W, Liu H, Zhang M, Xu T, Si C (2021) Cellulose nanomaterials for oil exploration applications. *Polym Rev* 1–41. <https://doi.org/10.1080/15583724.2021.2007121>
  50. Liu K, Du H, Zheng T, Liu H, Zhang M, Zhang R, Li H, Xie H, Zhang X, Ma M, Si C (2021) Recent advances in cellulose and its derivatives for oilfield applications. *Carbohydr Polym* 259:117740. <https://doi.org/10.1016/j.carbpol.2021.117740>
  51. Li L, Wu Z, Liang J, Yu L (2020) Application of deep eutectic solvents in lignocellulosic biomass processing. *J For Eng* 5(4):20–28. <https://doi.org/10.13360/j.issn.2096-1359.201907035>
  52. Tong C, Chen N, Ru J, Shan P, Liu H, Du C (2020) The influence of PFI pretreatment on physicochemical characteristics of cationic nanofibrillated cellulose prepared from once-dried and never-dried bamboo pulps. *J For Eng* 5(2):82–89. <https://doi.org/10.13360/j.issn.2096-1359.201907036>
  53. Wang X, Tang S, Wu Z, Fang J, Qin X, Wei L (2021) Research status of biomass-based composite films with high barrier properties. *J For Eng* 6(6):13–22. <https://doi.org/10.13360/j.issn.2096-1359.202102002>
  54. Miao C, Du H, Zhang X, Tippur HV (2021) Dynamic crack initiation and growth in cellulose nanopaper. *Cellulose*. <https://doi.org/10.1007/s10570-021-04310-x>
  55. Miao C, Du H, Parit M, Jiang Z, Tippur HV, Zhang X, Liu Z, Li J, Wang R (2020) Superior crack initiation and growth characteristics of cellulose nanopapers. *Cellulose* 27(6):3181–3195. <https://doi.org/10.1007/s10570-020-03015-x>
  56. Wu J, Che X, Hu H, Xu H, Li B, Liu Y, Li J, Ni Y, Zhang X, Ouyang X (2020) Organic solar cells based on cellulose nanopaper from agroforestry residues with an efficiency of over 16% and effectively wide-angle light capturing. *J Mater Chem A* 8(11):5442–5448. <https://doi.org/10.1039/C9TA14039E>
  57. Parit M, Du H, Zhang X, Prather C, Adams M, Jiang Z (2020) Polypyrrole and cellulose nanofiber based composite films with improved physical and electrical properties for electromagnetic shielding applications. *Carbohydr Polym* 240:116304. <https://doi.org/10.1016/j.carbpol.2020.116304>
  58. Liu H, Xu T, Cai C, Liu K, Liu W, Zhang M, Du H, Zhang K, Si C. (2022) Multifunctional superelastic, superhydrophilic, and ultralight nanocellulose-based composite carbon aerogels for compressive supercapacitor and strain sensor. *Adv Funct Mater* 32:2113082. <https://doi.org/10.1002/adfm.202113082>
  59. Du H, Liu W, Zhang M, Si C, Zhang X, Li B (2019) Cellulose nanocrystals and cellulose nanofibrils based hydrogels for biomedical applications. *Carbohydr Polym* 209:130–144. <https://doi.org/10.1016/j.carbpol.2019.01.020>
  60. Ma W, Li L, Xiao X, Du H, Ren X, Zhang X, Huang T-S (2020) Construction of chlorine labeled ZnO–chitosan loaded cellulose nanofibrils film with quick antibacterial performance and prominent UV stability. *Macromol Mater Eng* 305(8):2000228. <https://doi.org/10.1002/mame.202000228>
  61. Du X, Zhang Z, Liu W, Deng Y (2017) Nanocellulose-based conductive materials and their emerging applications in energy devices - a review. *Nano Energy* 35:299–320. <https://doi.org/10.1016/j.nanoen.2017.04.001>
  62. Liu H, Xu T, Liang Q, Zhao Q, Zhao D, Si C. (2022) Compressible cellulose nanofibrils/reduced graphene oxide composite carbon aerogel for solid-state supercapacitor. *Adv Compos Hybrid Mater*. <https://doi.org/10.1007/s42114-022-00427-0>
  63. Yang J, Li H, Cheng J, He T, Li J, Wang B (2021) Nanocellulose intercalation to boost the performance of MXene pressure sensor for human interactive monitoring. *J Mater Sci* 56(24):13859–13873. <https://doi.org/10.1007/s10853-021-05909-y>
  64. Zhu M, Wu J, Du Z, Tay RY, Li H, Özyilmaz B, Teo EHT (2015) A wafer-scale graphene and ferroelectric multilayer for flexible and fast-switched modulation applications. *Nanoscale* 7(35):14730–14737. <https://doi.org/10.1039/C5NR03020J>
  65. Cao W, Chen F, Zhu Y, Zhang Y, Jiang Y, Ma M, Chen F (2018) Binary strengthening and toughening of MXene/cellulose nanofiber composite paper with nacre-inspired structure and superior electromagnetic interference shielding properties. *ACS Nano* 12(5):4583–4593. <https://doi.org/10.1021/acsnano.8b00997>
  66. Zhang S, Liu H, Yang S, Shi X, Zhang D, Shan C, Mi L, Liu C, Shen C, Guo Z (2019) Ultrasensitive and highly compressible piezoresistive sensor based on polyurethane sponge coated with a cracked cellulose nanofibril/silver nanowire layer. *ACS Appl Mater Interfaces* 11(11):10922–10932. <https://doi.org/10.1021/acsaami.9b00900>
  67. Lee T-W, Lee S-E, Jeong YG (2016) Highly effective electromagnetic interference shielding materials based on silver nanowire/cellulose papers. *ACS Appl Mater Interfaces* 8(20):13123–13132. <https://doi.org/10.1021/acsaami.6b02218>
  68. Chen S, Carroll DL (2002) Synthesis and characterization of truncated triangular silver nanoplates. *Nano Lett* 2(9):1003–1007. <https://doi.org/10.1021/ml025674h>
  69. Lu L, Wei X, Zhang Y, Zheng G, Dai K, Liu C, Shen C (2017) A flexible and self-formed sandwich structure strain sensor based on AgNW decorated electrospun fibrous mats with excellent sensing capability and good oxidation inhibition properties. *J Mater Chem C* 5(28):7035–7042. <https://doi.org/10.1039/C7TC02429K>
  70. Priyadarshi R, Negi YS (2019) Poly(vinyl pyrrolidone)-mediated synthesis of silver nanowires decorated with silver nanospheres and their antimicrobial activity. *Bull Mater Sci* 42(3):118. <https://doi.org/10.1007/s12034-019-1779-3>
  71. Du H, Liu C, Mu X, Gong W, Lv D, Hong Y, Si C, Li B (2016) Preparation and characterization of thermally stable cellulose

- nanocrystals via a sustainable approach of  $\text{FeCl}_3$ -catalyzed formic acid hydrolysis. *Cellulose* 23(4):2389–2407. <https://doi.org/10.1007/s10570-016-0963-5>
72. Du H, Liu C, Zhang Y, Yu G, Si C, Li B (2016) Preparation and characterization of functional cellulose nanofibrils via formic acid hydrolysis pretreatment and the followed high-pressure homogenization. *Ind Crops Prod* 94:736–745. <https://doi.org/10.1016/j.indcrop.2016.09.059>
73. Xie H, Zou Z, Du H, Zhang X, Wang X, Yang X, Wang H, Li G, Li L, Si C (2019) Preparation of thermally stable and surface-functionalized cellulose nanocrystals via mixed  $\text{H}_2\text{SO}_4$ /Oxalic acid hydrolysis. *Carbohydr Polym* 223:115116. <https://doi.org/10.1016/j.carbpol.2019.115116>
74. Du H, Parit M, Wu M, Che X, Wang Y, Zhang M, Wang R, Zhang X, Jiang Z, Li B (2020) Sustainable valorization of paper mill sludge into cellulose nanofibrils and cellulose nanopaper. *J Hazard Mater* 400:123106. <https://doi.org/10.1016/j.jhazmat.2020.123106>
75. Hong S, Song Y, Yuan Y, Lian H, Liimatainen H (2020) Production and characterization of lignin containing nanocellulose from luffa through an acidic deep eutectic solvent treatment and systematic fractionation. *Ind Crops Prod* 143:111913. <https://doi.org/10.1016/j.indcrop.2019.111913>
76. Wang H, Xie H, Du H, Wang X, Liu W, Duan Y, Zhang X, Sun L, Zhang X, Si C (2020) Highly efficient preparation of functional and thermostable cellulose nanocrystals via  $\text{H}_2\text{SO}_4$  intensified acetic acid hydrolysis. *Carbohydr Polym* 239:116233. <https://doi.org/10.1016/j.carbpol.2020.116233>
77. Luan VH, Tien HN, Cuong TV, Kong B-S, Chung JS, Kim EJ, Hur SH (2012) Novel conductive epoxy composites composed of 2-D chemically reduced graphene and 1-D silver nanowire hybrid fillers. *J Mater Chem* 22(17):8649–8653. <https://doi.org/10.1039/C2JM16910J>
78. Lv P, Zhou H, Zhao M, Li D, Lu K, Wang D, Huang J, Cai Y, Lucia LA, Wei Q (2018) Highly flexible, transparent, and conductive silver nanowire-attached bacterial cellulose conductors. *Cellulose* 25(6):3189–3196. <https://doi.org/10.1007/s10570-018-1773-8>
79. Wan Y, Xiong P, Liu J, Feng F, Xun X, Gama FM, Zhang Q, Yao F, Yang Z, Luo H, Xu Y (2021) Ultrathin, strong, and highly flexible  $\text{Ti}_3\text{C}_2\text{T}_x$  MXene/bacterial cellulose composite films for high-performance electromagnetic interference shielding. *ACS Nano* 15(5):8439–8449. <https://doi.org/10.1021/acsnano.0c10666>
80. Zeng Z, Wu T, Han D, Ren Q, Siqueira G, Nyström G (2020) Ultralight, flexible, and biomimetic nanocellulose/silver nanowire aerogels for electromagnetic interference shielding. *ACS Nano* 14(3):2927–2938. <https://doi.org/10.1021/acsnano.9b07452>
81. Wei H, Wang M, Zheng W, Jiang Z, Huang Y (2020) 2D  $\text{Ti}_3\text{C}_2\text{T}_x$  MXene/aramid nanofibers composite films prepared via a simple filtration method with excellent mechanical and electromagnetic interference shielding properties. *Ceram Int* 46(5):6199–6204. <https://doi.org/10.1016/j.ceramint.2019.11.087>
82. Wen B, Cao M, Lu M, Cao W, Shi H, Liu J, Wang X, Jin H, Fang X, Wang W, Yuan J (2014) Reduced graphene oxides: light-weight and high-efficiency electromagnetic interference shielding at elevated temperatures. *Adv Mater* 26(21):3484–3489. <https://doi.org/10.1002/adma.201400108>
83. Miao M, Liu R, Thaiboonrod S, Shi L, Cao S, Zhang J, Fang J, Feng X (2020) Silver nanowires intercalating  $\text{Ti}_3\text{C}_2\text{T}_x$  MXene composite films with excellent flexibility for electromagnetic interference shielding. *J Mater Chem C* 8(9):3120–3126. <https://doi.org/10.1039/C9TC06361G>
84. Xin W, Xi G, Cao W, Ma C, Liu T, Ma M, Bian J (2019) Light-weight and flexible MXene/CNF/silver composite membranes with a brick-like structure and high-performance electromagnetic-interference shielding. *RSC Adv* 9(51):29636–29644. <https://doi.org/10.1039/C9RA06399D>

**Publisher's Note** Springer Nature remains neutral with regard to jurisdictional claims in published maps and institutional affiliations.